



**HAL**  
open science

# Multi-scale mechanical behaviour of a gothic monument composed of ashlar masonry. Application to the design of a reinforcement technique

Thomas Parent, Nathalie Domede, Alain Sellier

## ► To cite this version:

Thomas Parent, Nathalie Domede, Alain Sellier. Multi-scale mechanical behaviour of a gothic monument composed of ashlar masonry. Application to the design of a reinforcement technique. International Journal of Architectural Heritage, 2016, 11 (3), pp.399-414. 10.1080/15583058.2016.1238970 . hal-02005567

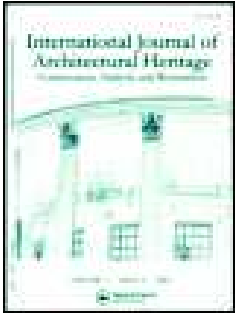
**HAL Id: hal-02005567**

**<https://hal.science/hal-02005567>**

Submitted on 4 Feb 2019

**HAL** is a multi-disciplinary open access archive for the deposit and dissemination of scientific research documents, whether they are published or not. The documents may come from teaching and research institutions in France or abroad, or from public or private research centers.

L'archive ouverte pluridisciplinaire **HAL**, est destinée au dépôt et à la diffusion de documents scientifiques de niveau recherche, publiés ou non, émanant des établissements d'enseignement et de recherche français ou étrangers, des laboratoires publics ou privés.



# Multi-Scale Mechanical Behavior of a Gothic Monument Composed of Ashlar Masonry. Application to the Design of a Reinforcement Technique

T. Parent, N. Domede & A. Sellier

**To cite this article:** T. Parent, N. Domede & A. Sellier (2016): Multi-Scale Mechanical Behavior of a Gothic Monument Composed of Ashlar Masonry. Application to the Design of a Reinforcement Technique, *International Journal of Architectural Heritage*, DOI: [10.1080/15583058.2016.1238970](https://doi.org/10.1080/15583058.2016.1238970)

**To link to this article:** <http://dx.doi.org/10.1080/15583058.2016.1238970>



Accepted author version posted online: 11 Oct 2016.



Submit your article to this journal [↗](#)



View related articles [↗](#)



View Crossmark data [↗](#)

# Multi-scale mechanical behavior of a gothic monument composed of ashlar masonry. Application to the design of a reinforcement technique

T. Parent<sup>\*,\*\*</sup>, N. Domede<sup>\*</sup>, A. Sellier<sup>\*</sup>

<sup>\*</sup>Université de Toulouse; UPS, INSA; LMDC (Laboratoire Matériaux et Durabilité des Constructions) ; 135, avenue de Rangueil ; F-31 077 Toulouse Cedex 04, France

<sup>\*\*</sup>Corresponding author (Mel: parent@insa-toulouse.fr)

## Abstract

This paper presents a structural method for the assessment of a gothic monument composed of buttresses and ribbed vaults. The FEM approach used is based on identifying a working point that corresponds to an equilibrium state of the structure. It leads to the design of a strengthening solution for the structure. The multi scale approach begins at the component scale with the determination of the mechanical properties of the masonry from sound velocity measurements. Then a homogenization method is used to preserve the heterogeneous character of the masonry at the structural scale. A failure criterion is developed that takes account of the complex failure modes of masonry subjected to axial and bending loads and of the uncertainties on its mechanical characteristics. Finally, the effectiveness of this approach for designing a strengthening solution is presented and discussed.

**KEY WORDS:** Gothic vault, Masonry, FEM, Damage modelling, Homogenization, Crack

## Introduction

France has about 40 000 buildings that are classified as historical monuments. The work presented here was carried out in the context of the preservation of this architectural heritage. It focuses on developing a tool to support decision-making in the reinforcement of Gothic masonry structures. Understanding the structural behaviour of Gothic monuments is a challenge for the architects, engineers and archaeologists in charge of protecting and preserving our architectural heritage. The complexity of the buildings' geometry, the restriction on destructive tests in situ, and the lack of knowledge of the construction principles are all factors that make the study of mediaeval monuments delicate. Moreover, because each historical monument is unique, 6 principal elements have to be taken into consideration when studying it [1][2]: (a) the building's history, (b) ancient materials, (c) the geometry of the structure, (d) its morphology and connections, (e) Actions, and (f) damage and degradation.

The final aim of the present work is to make a structural analysis of a 13th century gothic building so that a solution can be designed for repairing the structure. Structures of this kind consist of two major components: ribbed vaults and structural walls with buttresses. Connecting these two elements are the supports of the vault, and the load due to the self-weight of the vault is necessarily transmitted to the wall by the supports. The structural analysis consists of finding an equilibrium state point called the "working point" of the vault/buttress system. This equilibrium depends on two interconnected phenomena: horizontal load on the supports of the vault and the horizontal displacement of the buttresses. The overall stability depends on the rigidity of these two slender elements.

To establish the working point, the behaviour laws for horizontal load vs. horizontal displacement need to be determined for the two elements, vault and buttress. These two structures are composed of limestone blocks bonded by thin lime mortar. This ancient material shows strong non-linearity, heterogeneity and anisotropy. Since Coulomb first proposed his theory, many calculation methods have been developed to describe the mechanical behaviour of masonry structures at different scales [3][4]. Today, there are 3 principal numerical methods: the analytical method (elastic or plastic) [5][6], the distinct element method (DEM) [7][8][9] and the finite element method (FEM). The FEM method used in the present work has previously served for the structural analysis of Mallorca cathedral [10] and the failure analysis of the Monastery of Jerónimos [11]. It allows the heterogeneous, non-linear character of the masonry to be considered while preserving the simplicity of the calculation through a homogenized approach. The homogenization approach has already been used by the authors to estimate the load bearing capacity of masonry vault bridges, which are massive elements. Here, the elements of the monument under study are slender, so the method is refined for the assessment of slender masonry elements and to handle the diverse loading section (axial load, bending moment, and both). The continuum damage model developed by the authors and used in this work includes crack localization and therefore considers induced orthotropic damage [12]. It allows the structural behaviour to be assessed while considering the pathologies observed on the structure (crack pattern).

In the following sections, first, the monument will be described, with the architectural particularities of the building, the observed pathologies and the different elements and zones making up the structure. Then, a sound-velocity campaign, carried out on the limestones blocks

in order to estimate the mechanical properties of the masonry in place, will be presented. The fourth section deals with the multi-scale study of the masonry material. A failure criterion will be developed that takes account of (a) the complex failure modes of the masonry and (b) the uncertainties on the mechanical properties of limestones. Then, we will develop the global method for estimating the safety margin of the structure by using the working point and the observed crack patterns. Finally, the design of a repair solution for the structure will be presented and discussed.

## **The monument**

### **Architecture**

The methodology presented in this work is based on the structural assessment of a gothic monument located in the 3rd district of Paris. This building was initially a monks' refectory and, today, is a university library. It was built in 1230. The interior and exterior views are shown in Figure 1 (a) and (b). The building has a length of 43 m and a width of 11.4 m. It is considered as one of the masterpieces of Gothic architecture [15]. Slender buttresses located outside divide the monument into eight bays. Seven isolated columns are situated along the longitudinal axis of the building. Figure 1 (e) shows a plan view of the monument. It was drawn by the chief architect in charge of France's historic monuments, who is also the person in charge of the library. The lateral and gable walls are respectively the elevation walls parallel and perpendicular to the axis of the nave. In this work, the bays are designated by numbers that increase from east to west (1 to 8).

Transversal section of Figure 1(d) indicates the arrangement of the two rows of ribbed vaults. This cross sectional view is taken on the second bays and is oriented towards the east. The section plane is at the level of the two keystones of the ribbed gothic vaults. This figure also shows the slender column that divides the two rows of ribbed vaults. The roofing framework can also be identified on the figure. It dates from the construction period and is one of the oldest timber roof frames in Paris. It is composed of nine trusses: two extreme trusses over the gable walls and seven intermediary trusses above the buttresses, which is a typical Parisian roof frame of the 13th century. This roofing framework of “rafters that form the truss” may apply a horizontal thrust to the lateral walls.

The transversal cross sectional view of the library shows the arrangement of the vaults in the longitudinal direction Figure 1 (c). The distance between the columns is not constant. Bay 6 is wider than the others and bay 5 is smaller. According to the chief architect of historical monuments in charge of the building, these deviations were certainly motivated by some "local difficulties of construction" [14]. This particular arrangement is also highlighted on the plan (Figure 1(e)).

### **Crack Pattern on intrados of vaults**

A complex crack pattern was observed on the intrados of the vaults (Figure 2), but common trends could be seen in all the bays. Longitudinal cracking under the panels extends from east to west on the two rows of ribbed vaults. These cracks are slightly offset from the keystones towards the outside. Their opening is about 0.3 mm on the crossed ribs and 1.5mm on the transverse arches. On the webs, the cracks do not exceed 0.1mm. Displacement gauges placed on

a large number of these cracks in 2006 indicated that the crack openings had not changed since this time.

## **Masonry**

The masonry in place in the building is made of limestone bonded with lime mortar and its conservation status inside is relatively good. The thickness of the bed mortars is less than 1.0 cm (average value: 0.9 cm, CV=52%). Five zones of masonry were identified: 2 for the buttress and 3 for the ribbed vault. Regarding the lateral and gable walls, 2 zones were defined: the basement level and the upper level. The first is between the soil and the base of the bay windows (Figure 3(a)). It seems to be composed of soft limestone. The second zone (upper level) rises from the base of bay to the top of the wall. It seems to be composed by softer limestone blocks (highest porosity visible to the naked eye). Those two ashlar fine masonries are made of limestone bonded with lime mortar.

Three zones were distinguished on the ribbed vault (Figure 3 (b)): (i) webs made of ashlar masonry, (ii) transverse and wall arches (made of the same ashlar masonry), and crossed ribs, having a cross smaller than the other two. The ribs are all composed by soft limestone blocks arranged in series and bonded by lime mortar. The thickness of the bed mortar is constant so the rib blocks have beveled edge to follow the vault curve.

# Velocity measurements of ultrasonic wave propagation

Ultrasonic testing is non-destructive and quickly provided extensive information on the quality of the limestone in place on the monument. The 5 zones identified in the previous paragraph were distinguished in the measurement campaign. For each zone, at least 3 blocks were tested. Measurements were indirect (at the visible surface of the block). For each limestone tested, 10 measurements of ultrasonic wave propagation were made. For each block tested, the average standard deviation of the 10 measurements was about 6%. This fact shows, firstly, that the auscultation technique is repeatable and, secondly, that the limestone is relatively homogeneous at the scale of the constituent blocks

Table 1 summarizes the whole non-destructive test campaign. For the elevation walls, it can be seen that the basement level gave a higher sound velocity than the upper level (respectively 2966 m/s and 2313 m/s). Concerning the vault, the sound velocity reached 2774 m/s for the panels, 2722 m/s for the crossed ribs and 3076 m/s for the transverse and wall arches. Moreover, the measurement dispersions for the block tested on the elevation wall (CV=25% for the basement wall and CV= 29% for the upper wall) shows that there is strong heterogeneity among the limestone blocks. In contrast, dispersion was lower for the vault zones, showing better homogeneity.

# **Homogenized behaviour of an ashlar masonry of limestone bonded with lime mortar**

Masonry is a heterogeneous, nonlinear, anisotropic material. This heterogeneous characteristic encourages the use of a homogenization method as it would be difficult and needlessly complicated to perform a nonlinear calculation at the scale of the structure by differentiating each real block and mortar in the mesh. For this reason, the study rather focuses on the use of a material that is homogeneous at the structural scale but has mechanical characteristics that are taken from the mechanical properties and the arrangement of the components of the masonry. The approach is based on the mechanical characterization of the constituent masonry elements (constituent scale) to rise progressively to the scale of the structure (macroscopic scale). The link between these two extreme scales is made by using a homogenization method at the mesoscopic scale. The calculation is presented according to the multi-scale approach: (i) constituent scale, (ii) mesoscopic scale (homogenization method) and (iii) structural scale. But before we describe this multi-scale method, the following paragraph presents the damage model used to simulate the behaviour of the geomaterials at each scale of study.

## **Orthotropic damage model**

It has been seen that the constituents of masonries forming the library are limestones bonded by lime mortar. These materials belong the family of geomaterials. This kind of materials presents complex mechanical behaviour: (a) Initial elastic law, (b) strength asymmetry in tension and

compression, (c) soft hardening in tension and compression, (d) loss of stiffness during the loading, resulting from the damage of material in tension and compression, (e) non-reversible plastic strain, (f) restitution of rigidity during crack reclosure and (g) sensitivity of the compressive strength to the confining pressure.

To consider the whole non-linear characteristics, an élasto-plastic orthotropic damage model is used [12] [15]. The material is not initially orthotropic but becomes so through crack propagation. The model was computed in the FEM software CAST3M. The constitutive law was formulated in the framework of thermodynamics. It is based on the strain equivalence principle. The damage law links the real stress tensor  $\sigma_{ij}$  to the effective stress tensor  $\tilde{\sigma}_{kl}$  which is separated into its positive part  $\tilde{\sigma}_{kl}^+$  (tension) and its negative parts  $\tilde{\sigma}_{kl}^-$  (compression) (Eq. 1). In this equation,  $D^S$  is shear and compression scalar damage,  $D_0^t$  is the post peak localized damage in direct tension and  $D^t$  is the orthotropic tension damage after the tension peak. Lastly,  $D^r$  represents compressive damage during crack re-closure.

$$\sigma_{ij} = (1 - D^S) [(1 - D_0^t)(1 - D^t)_{ijkl} \tilde{\sigma}_{kl}^+ + (1 - D^r)_{ijkl} \tilde{\sigma}_{kl}^-] \quad \text{Eq. 1}$$

The damage model presents plastic multi-criteria as shown in Figure 4. In compression, a Drucker-Prager criterion is computed. It offers the possibility to consider the influence of confining pressure on the compressive strength of the geomaterial. In tension, a Rankine criterion is applied. The orthotropic model allows the independent propagation and re-closure of 3 orthogonal cracks. It is based on the rotating crack method. Due to softening, tensile damage and compressive damage lead to localization of strains. The objectivity of the FEM solution

toward the mesh is processed with a Hillerborgh method [16]. To avoid dependency of the Hillerborgh method on the finite element shape, the model uses an anisotropic description of element size (TAILLE operator in CAST3M). A stiffness method based on restitution during any crack reclosure was also implemented [17]. An important point in this work is that the model allows the calculation of crack opening from the plastic strain in tension and the size of the mesh element concerned. Figure 5 shows the stress-strain law of the orthotropic model subjected to a tensile load and then a compressive load. The red curve indicates axial stress versus axial strain. Elastic pre-peak behaviour in tension can be observed at (1), peak tensile strength at (2), soft hardening in tension corresponding to the opening of the localized crack at (3), progressive crack re-closure at (4) during the transition from tension to compression according to [17], elastic behaviour in compression at (5), peak compressive strength at (6), soft hardening in compression at (7) with non-associated plastic flow. The volumetric strain (in green) shows the dilatancy of the plasticity model (8).

## **Microscopic scale**

The use of this model for limestone blocks and lime mortar requires the mechanical characteristics to be identified in tension and compression. However, two major difficulties are encountered in the mechanical characterization of the constitutive elements: (i) the historical and architectural aspect of the monument restrict the possibility of drilling cores, and (ii) the materials in place are heterogeneous whether it be at the scale of distinct zones of masonry or at the scale of the structure. For this reason, the proposed characterization method is based on the exploitation of sound velocity measurements introduced in the previous part.

Non-destructive measurement of the velocity of sound allows the mechanical characteristics of limestone blocks to be estimated from an empirical correlation law [18],[19]. Moreover, it is also possible to quantify the dispersion in the mechanical characteristics of limestone blocks at the masonry scale with this method. Preliminary research had been carried out in order to establish new correlation laws between the sound velocity measurement  $V_P$  and the mechanical characteristics of limestones namely: density  $\rho$ , compressive strength  $R_c$ , tensile strength  $R_t$ , elasticity modulus  $E$ , and Poisson ratio  $\nu$  [20]. The mechanical data used in this previous work came from a collection of international literature by 13 authors. Equation 2 shows for example the relationship between compressive strength  $R_c$  and sound velocity  $V_P$ . The standard deviation  $CV_{V_P}$  enable a probabilistic quantification of the error on the estimation of the compressive strength of the limestone blocks used in the construction of the library. Finally, Table 2 shows the principal mechanical characteristics of limestone blocks of each zone.

$$R_c = 5.61 * 10^{-9} V_p^{2.75} \quad (CV_{V_p}=34\%, R^2=0.86) \quad \text{Eq. 2}$$

Concerning bed mortars, it can be noted that, for medieval gothic, thin bed lime mortar was employed. At this time in history, stone was meticulously cut thanks to a mastery of stereotomy techniques and the proportion of mortar was small compared to the limestone blocks. In this configuration, the homogenized behaviour of masonry depends essentially on the blocks. Unfortunately, sound velocity measurement is difficult because of the thickness of the bed mortar. Moreover, the statistical data in the literature concerning the correlation between sound velocity and mechanical characteristics are rare.

So the mortar characteristics were estimated using an equivalent lime mortar made in the laboratory according to the formulations used in the Middle Ages [21], [22], [23]. The composition of the mortar was 300 kg of lime for 1 m<sup>3</sup> of sand. The lime was poorly hydraulic (NHL 3.5) according to the European standards [24]. Three point bending tests and a compressive test were performed on 4\*4\*16 cm<sup>3</sup> specimens [25]. These mechanical tests led to an estimation of the principal mechanical characteristics of lime mortars. Table 3 summarizes these properties. Thus, the mechanical properties of blocks and mortar were estimated for the 5 zones of masonry and it was possible to estimate the homogenized behaviour of the masonry at the mesoscopic scale.

### **Mesoscopic scale: homogenization**

From the mechanical and geometrical characteristics of the individual components of the masonries, it was possible to identify the mechanical characteristics of the homogenized material. The homogenization method used here had already been used by the authors to estimate the behaviour of a vaulted bridge [26] [27]. In tension, homogenized tensile strength corresponds to the strength of the block/mortar interface which is the weakest link of the masonry in tension. This tensile strength was identified by an experimental campaign of direct tension tests on 6 composite block-mortar-block specimens. The results of this measurement gave to a mean value  $R_t$  of about 0.05 MPa.

In compression, the homogenization for the five zones was done by a nonlinear simulation of a direct compressive test on a representative elementary volume (REV) according to the RILEM recommendation [28] (Figure 6). The basic assumptions of this “virtual laboratory test” are: (i)

the upper and lower faces of the wall are not blocked horizontally in order to keep isostatic conditions, (ii) the nodes at the interfaces mortar/block stay attached, ie there is no sliding between mortar and block, and (iii) the numerical compressive test is carried on in imposed displacement in order to estimate the post-pic behaviour of masonry.

This approach allowed the effect of the confined mortar to be evaluated with respect to the relative stiffness between mortar and limestone blocks. Figure 7 shows the experimental behaviour in compression of a Saint-Maximin limestone drilled from the library and the equivalent mortar formulated in the laboratory. Strong differences can be observed for (i) compressive strength (17 MPa for the block and 1.1 MPa for the mortar) and (ii) stiffness (9.3 GPa for the block and 0.15 GPa for mortar). The dotted curves shows the experimental results while the continuous curves are the curves fitted using of the damage model.

The red curve corresponds to the behaviour law in compression of the numerical REV wall subjected to an axial compressive load with imposed displacement. First of all, it can be seen that the compressive strength of the masonry (15 MPa) is close to the compressive strength of the limestone blocks (17 MPa). This highlights the effect of confinement on the mortar, which increases its compressive strength. This effect was expected because of the marked stiffness difference between mortar and blocks and the thickness of the bed mortar. Thus, in this case, the compressive strength of the mortar plays a negligible role in the compressive strength of the masonry and failure occurs by limestone crushing. The diminution of strength between block and masonry is the result of the presence of a peripheral area of unconfined mortar, which reduces the specific resistance section of the block and so the REV [20].

Compressive damage at the failure of the REV is shown in Figure 8(b). The peripheral area is indicated at ( $\alpha$ ). An experimental study carried on composite samples of block-mortar-block also showed the peripheral area Figure 8(a). Note that the confinement of bed mortar is indirectly observed on the blocks, which present vertical cracks (Figure 8(c)). The stiffness difference implies a triaxial compressive stress state in the mortar and a biaxial tensile stress state in the directions perpendicular to the load axis. These cracks ( $\beta$ ) were observed in the experimental test Figure 8(a) and in the numerical simulation Figure 8(c).

Finally, the red dotted curve shows the fitting procedure of the homogenized damage model on the response of REV in compression (Figure 7). It is thus possible to consider masonry as a homogeneous geomaterial and elasto-plastic damage model was used to consider all of the nonlinear phenomena of this meso-material

The homogenization method under axial load was carried out on five REV corresponding to the 5 zones of the library. The behaviour law in compression of each zone is shown in Figure 9. Several observations on the stiffnesses and strengths of different areas testify to the relevance of the choice of materials made by the Gothic builders. First of all, the masonry of the upper level is less resistant ( $R_c = 10\text{MPa}$ ) than the masonry of the basement level ( $R_c = 20\text{ MPa}$ ). This choice is relevant in so far as the most loaded section is at the base of the wall. Secondly, masonries of the buttresses are stiffer ( $E \approx 3000\text{ MPa}$ ) than in the arch ( $E \approx 1200\text{ MPa}$ ). This difference comes from the fact that masonries of the vault present a ratio  $r$  (bed mortar thickness to block height) higher than those of buttress. The Gothic builders were probably aware that the use thick bed mortar and low-height blocks for the vaults would decrease the stiffness of the composite

material "masonry". However, the vault must be able to adapt to horizontal displacement of the supports and this adaptation is easier when the masonry is flexible. Finally, we note that increasing the ratio  $r$  for vaults does not lead to a decrease of the compressive strength of the masonry. Mortar is indeed sufficiently confined and so the rupture occurs by reaching the peak of compression in the limestone blocks.

### **Homogenized failure criterion of the damage model**

The homogeneous model obtained in the previous section can be used to conduct a calculation at structural scale. However, when a vault is subjected to variations of boundary conditions, axial and bending loads are observed in some sections and a crack may propagate on the tensioned fibre when the eccentricity of the normal load is out of the middle third. The structure adapts to these changes by creating plastic hinges, decreasing its degree of indeterminacy. It is in the block-mortar interfaces, the weakest area of the masonry, that cracks may open. Thus, the effective surface area of the cracked section decreases, which causes concentrations of compressive normal stress when the element is subjected to an axial and bending load. The use of a homogeneous scale model of the structure allows the progressive decrease of the tensile normal stresses to be taken into account in the cracked zone. However, if no precautions are taken, the homogenized model overestimates the compressive strength of masonry at the cracked sections.

## Homogenized criterion in bending and axial load.

To understand and identify the failure behaviour of a masonry section under complex loading, a numerical test was carried out on a mesh consisting of a bed mortar and a limestone block (Figure 10). Three distinct boundary conditions were applied with an imposed displacement of the mortar surface along the  $y$  axis: (a) uniform displacement on the whole height of the mortar, (b) triangular displacement on the total height of the mortar and (c) triangular displacement on the third of the height. The latest case is chosen to simulate a bending and axial load on a cracked section of masonry.

Figure 10 shows firstly the normal stress variation along the  $z$  axis when the failure occurs. The load case (a) leads to a relatively uniform state of normal stress and equal to the compressive strength of the block and thus approximately to the compressive strength of masonry. Nevertheless, a decrease of the normal stress is observed at the upper and lower fibres. This decrease corresponds to the peripheral area of the un-confined mortar previously presented and explains the lower compressive strength of ashlar thick bed mortar masonry in comparison with the limestone block. Furthermore, it can be seen that when the load approaches a bending and axial load with a cracked section (case (c)), the normal stress diagram at failure takes the form of an isosceles bi-triangular diagram. This phenomenon is explained by the strength loss of the mortar which is not confined to the top compressed fibre. It can also be noted that as well as the normal load taking away the neutral fibre, the proportion of confined mortar decreases, which causes a decrease in the average strength of the section.

Figure 11 shows the compressive-shear damage of the numerical test for the 3 cases of loading at the failure of the section. The peripheral area of unconfined damaged mortar is highlighted in (a) in the case of simple axial load. It is at this band that there is compression damage of up to about 0.7 in the corners of the section. When the eccentricity of the normal load increases (cases (b) and (c)), the peripheral area progressively concentrates at the compressed fibre and compressive damage become greater. In those cases the mortar is not confined uniformly and the average compressive strength decreases progressively.

These complex phenomena observed at mesoscopic scale are not considered at the structural scale in the homogenized material, whose compressive centered strength is  $R_{c,H}$ . The homogenized model overestimates the compressive strength when the load is eccentric (bending and axial load). To take account of this mechanical phenomenon while preserving the homogenous character of the model, a failure criterion is proposed. A working coefficient  $\chi^d$  such that  $\sigma_{Max} < \chi^d R_{c,H}$  where  $\sigma_{Max}$  is the normal active stress obtained with the calculation at the structural scale and  $R_{c,H}$  the compressive centered strength obtained by the homogenization method at the mesoscopic scale. This coefficient depends on the eccentricity of the load and it is calculated by considering the ratio between the area normal stress diagrams of the homogenous material (structural scale) with diagram area a failure of the composite computed at the mesoscopic scale.

### 2.3.2. Consideration of the uncertainties on mechanical characteristics

The second aspect of the proposed criterion concerns the passage from a deterministic model to a probabilistic model. A partial safety factor  $\gamma_m$  is introduced such that  $R_{Ed} = R_{c,H}/\gamma_m$ .  $R_{Ed}$  is the design compressive strength. This factor takes two sources of uncertainty into account. The first concerns the use of correlation curves in the estimation of the strength of limestone and is computed from the standard deviation  $CV_{Vp}$  of the correlation law introduced in Eq 1. The second concerns the dispersion of sound velocity measurements in each of the 5 masonry zones. It is calculated from the standard deviation of sound velocity measurements on blocks for each zone (Table 3). So the partial safety factor depends on the area considered and will increase with the dispersion of measurements. The determination of the partial safety factor  $\gamma_m$  is based on the calculation of the mean and standard deviation of a random variable of the compressive strength of masonry  $R_{c,H}^a$ . The two uncertainties  $Err_{VP}$  and  $Err_{RC}$  previously introduced generate the randomness of this variable (Eq. 3).

$$R_{c,H}^a = R_{c,H} * Err_{VP} * Err_{RC} \quad \text{Eq. 3}$$

$$R_{Ed} = E(R_{c,H}^a) * e^{-\alpha\beta V} \quad \text{avec } V = \frac{\sqrt{VAR(R_{c,H}^a)}}{E(R_{c,H}^a)} \quad \text{Eq. 4}$$

The calculation of the variance  $VAR(R_{c,H}^a)$  and the average  $E(R_{c,H}^a)$  is based on the hypothesis that the variables  $R_{c,H}^a$ ,  $Err_{VP}$  et  $Err_{RC}$  follow a log-normal distribution law [20]. Table C3 of the

European standard (Eurocode 0) indicates how to calculate the design strength  $R_{Ed}$  of a variable that follow a log-normal law. This value depends on the average  $E(R_{c,H}^a)$ , the variance  $VAR(R_{c,H}^a)$  and two other coefficients  $\alpha$  and  $\beta$  (Eq. 4).  $\alpha$  is chosen equal to 1 according to the safety direction and  $\beta$  depends on the class of consequence of table B.1 of Eurocode 0 (For a historical monument, CC3 index) and on the reference time period (Table B.2, Eurocode 0). In this hypothesis,  $\beta=5.2$ .

We know that  $E(R_{c,H}^a) = R_{c,H}$  so it is possible to estimate the partial safety factor  $\gamma_m$  for each masonry zone (Eq. 5).

$$\gamma_m = \frac{R_{c,H}}{R_{Ed}} = e^{\alpha\beta V} \quad \text{Eq. 5}$$

Thus the criterion developed in this work takes account of the complex failure modes of a cracked section and the uncertainties on the compressive strength of masonries in Eq. 6.

$$\sigma_{Max} < \chi^d \frac{R_{c,H}}{\gamma_m} \quad \text{Eq. 6}$$

# Analysis of a gothic monument bay, structural scale

## Approach

The objective of the analysis presented here is to assess the safety margin concerning the failure of this structure in order to conclude on whether the observed disorders have a prejudicial character or not. Simplified mechanical modelling of a bay is shown Figure 12. It shows that (i) the vault BDE, the central part of which is supported by the column (sufficiently stiff along the z axis to block the vertical displacement of vault support E) and (ii) the buttress ABC on the outside of the building. When the centring is removed, the self-weight of the vault causes a horizontal load  $\vec{F}_H$  to appear at the vault supports. This load is transmitted through the tas-de-charge to the buttress, leading to a deflection of the buttress by bending and foundation rotation. The vault supports deviate each other. Thus, to adapt to this variation of boundary conditions, a crack pattern will appear on the vault. The vaults adapt to these changes by creating plastic hinges decreasing the degree of indeterminacy. Two failure modes can be highlighted: (i) failure of the vault itself by reaching a critical limit for horizontal displacement, for which the vault is no longer in static equilibrium and (ii) buttress failure by reaching a horizontal load leading to the overthrow of the buttress.

To solve the problem, the proposed method studies the behaviour of the vault and the buttress independently. The green and blue curves in Figure 13 are the typical relationships for horizontal load vs horizontal displacement of the buttress and the vault respectively. The horizontal limit  $F_{cri}$  is the load which leads to the failure of the buttress and the vertical limit  $\delta_{cri}$  is the

critical horizontal displacement leading to intrinsic vault failure. Three cases can be envisaged: the first is based on the assumption that if the two behaviour law intersect (case 1), then the system is in an equilibrium state and the intersection point  $P_f$  is called the working point. Otherwise, vault failure (case 2) or buttress failure (case 3) can be observed. So it the numerical study of the working point of a bay of the library will be presented while determining the vault and the buttress behaviour laws independently. Safety margins are then determined using the probabilistic criterion presented above.

## **Working point analysis**

### **Mesh**

Meshes of the ribbed vault and buttress are presented in Figure 14. The vault is made up of the crossed rib, the transverse and wall arches and the webs (Figure 14(a)). The buttress is composed of upper level and basement level masonries, foundations and an elastic soil (Figure 14(b)). The two meshes are made of cubic elements (CUB8 in CASTEM). This type of element allows the use of an operator (TAILLE) to compute the anisotropic size of each element in order to reach a Hillerborg local regularization in tension [16].

### **Mechanical characteristics of masonries**

The masonry material model is the homogeneous damage model presented in the first part of the paper. Each zone has its own characteristics, given by the sound velocity measurement and the homogenization process.

## **Loading step**

Concerning the vault, the load is applied in two steps: (a) progressive increase of the self-weight with blocked horizontal displacement of vault supports and (b) constant real self-weight and progressive increase of the horizontal displacement of vault supports. Concerning the buttress, the loading history of the library according to the ancient construction techniques was taken into account by successively applying: (a) self-weight of the buttress, (b) self-weight of the roof, (c) self-weight of the vault until its actual state and (d) increase of the horizontal load of the vault until buttress failure.

## **Behaviour law of vault and buttress**

The behaviour law (horizontal load vs horizontal displacement at the vault support) of the vault is presented in Figure 15. The first loading step (1) corresponds to increasing of the self-weight. The horizontal load reaches 20 kN at the end of step (2). Then, a phase can be observed where the load decreases progressively to an asymptote at 12 kN when the displacement increases (3). This decrease is due to the energy required to propagate the cracks presented in Figure 16. The system tends to progressively decrease its degree of indeterminacy and leads to a quasi-isostatic system. The method to determine the actual state of the vault consists of comparing the crack openings measured in situ and the numerical crack obtained by the modelling. Figure 16 shows the crack opening for an imposed displacement of the vault support of 1.5 cm. This displacement leads to a crack opening of 1.5 mm on the transverse arches. This opening corresponds to the opening measured on the intrados of the vault library. Thus, from this comparison, it is possible to estimate the actual stress state of the vault and so the real horizontal load supported by the

buttress (point (4) on the curve: 12.7 kN). From this state, cartography of the safety factor can be plotted. The safety factor at each point is found by calculating the ratio of the active normal stress  $\sigma_{Max}$  to the design compressive strength  $\chi^d \frac{R_{c,H}}{\gamma_m}$ . The most exposed failure zone is observed at the intrados of the transverse arches near to the support, with a value of 5.

The behaviour law of the buttress shows that the real loading of the vault (12.7 kN) leads to a displacement of the vault support of about 1 cm (Figure 17). For this state, the beginning of an opening crack can be observed at the internal and lower part of the buttress (Figure 18). It is in this cracked and most stressed section that the safety factor lowest reaching 2.

### **Working point analysis**

The global structural assessment of the bay is carried on by superposition of the two behaviour laws (Figure 19). The working point corresponds to the load/displacement (13 kN, 9 mm) pair. It is close to the point obtained by comparison of the crack opening. The difference can be explained by mortar creep (not considered in the analysis) or an overestimation of the horizontal stiffness at the vault support (due to an overestimation of the soil stiffness and/or an overestimation of the buttress stiffness). However, from a structural point of view, this difference does not call the proposed analysis into question. It can be said that the probabilistic safety margin is 2 for the buttress and 5 for the vault.

Finally, this working point analysis leads to conduct a simplified design of a strengthening solution (Figure 20). It consists of choosing a system that is a sufficiently stiff to prevent a limit displacement  $\delta_{lim}$  (arbitrarily defined as 7 cm in this example). The stiffness of the

strengthening solution is chosen by considering that the intersection of the Hook's law of the repair solution with the behaviour law of the vault present a relative displacement  $\delta_{cri}$  of about 1 cm. Then, the stiffness of the system is estimated at 13 kN/cm. We can suppose that, under the horizontal load of the vault, the displacement of the vault support increases. The causes of this additional movement could be the reduction of the mechanical properties of masonry by physico-chemical degradation or, a decrease of soil mechanical properties (by variation of the height of the water table). Then, progressively, the horizontal load of the vault will be transmitted in the repair solution instead of the buttress until the working point  $P_{f,2}$ . This point corresponds to the case where the buttress is no longer subjected to any horizontal force of the vault. In this case, the horizontal movement remains locked to this value. The repair system is rigid enough to block the displacement. We see here that the strengthening solution must be defined in terms of stiffness and not in terms of strength.

## Conclusion

A multi scale method for analysing ancient structures made of masonry has been presented in his article. The materials composing the structure were characterized by means of on-site measurements of the velocity of sound in the limestone blocks. Correlation curves were used to estimate the mechanical properties of the limestone of each masonry zone of the library. A nonlinear homogenization was used to identify the homogeneous characteristics of masonry. This approach enabled the transition to be made between the constituent scale and the structural scale. The use of an orthotropic damage model at each scale allowed (i) the complex failure phenomena of the masonry to be taken into account and (ii) on site measurements to be

compared with computed crack opening. However, the use of this model causes a loss of information on the complex failure modes of masonry subjected to an axial and bending load. A strength criterion is proposed to consider local failure modes of masonry under various loads while preserving a homogeneous model at the global scale of the structure. This criterion also takes the uncertainties on the mechanical characteristics of masonry into account by integrating a probabilistic character in the deterministic homogenized model. Finally, working point analysis is a simple method and keeps the possibility of designing the stiffness of the strengthening system

## **Bibliography**

- [1] P. Roca, M. Cervera, G. Gariup, and L. Pela', « Structural Analysis of Masonry Historical Constructions. Classical and Advanced Approaches », *Arch. Comput. Methods Eng.*, vol. 17, n° 3, p. 299-325, sept. 2010.
- [2] ICOMOS, « Recommendations for the analysis, conservation and structural restoration of architectural heritage », 2003.
- [3] P. Lourenço, G. Milani, A. Tralli, and A. Zucchini, « Analysis of masonry structures : review of and recent trends in homogenization techniques », nov. 2007.
- [4] P. Roca and G. Araiza, « Shear response of brick masonry small assemblages strengthened with bonded FRP laminates for in-plane reinforcement », *Constr. Build. Mater.*, vol. 24, n° 8, p. 1372-1384, août 2010.
- [5] P. Block and J. Ochsendorf, « Lower-bound Analysis of Masonry Vaults ». 2008.

- [6] J. Heyman, « The stone skeleton », *Int. J. Solids Struct.*, vol. 2, n° 2, p. 249-279, avr. 1966.
- [7] A. Rafiee, M. Vinches, and C. Bohatier, « Modelling and analysis of the Nîmes arena and the Arles aqueduct subjected to a seismic loading, using the Non-Smooth Contact Dynamics method », *Eng. Struct.*, vol. 30, n° 12, p. 3457-3467, déc. 2008.
- [8] V. H. Tran, E. Vincens, J. C. Morel, F. Dedecker, and H. H. Le, « 2D-DEM modelling of the formwork removal of a rubble stone masonry bridge », *Eng. Struct.*, vol. 75, p. 448-456, sept. 2014.
- [9] A. R. Tóth, Z. Orbán, and K. Bagi, « Discrete element analysis of a stone masonry arch », *Mech. Res. Commun.*, vol. 36, n° 4, p. 469-480, juin 2009.
- [10] P. Roca, M. Cervera, L. Pelà, R. Clemente, and M. Chiumenti, « Continuum FE models for the analysis of Mallorca Cathedral », *Eng. Struct.*, vol. 46, p. 653-670, janv. 2013.
- [11] P. B. Lourenço, K. J. Krakowiak, F. M. Fernandes, and L. F. Ramos, « Failure analysis of Monastery of Jerónimos, Lisbon: How to learn from sophisticated numerical models », *Eng. Fail. Anal.*, vol. 14, n° 2, p. 280-300, mars 2007.
- [12] A. Sellier, G. Casaux-Ginestet, L. Buffo-Lacarrière, and X. Bourbon, « Orthotropic damage coupled with localized crack reclosure processing. Part I: Constitutive laws », *Eng. Fract. Mech.*, vol. 97, n° 0, p. 148-167, janv. 2013.
- [13] V. Brunelle, Cabinet Cizel, and Ginger CEBTP, « CNAM, Ancien réfectoire, Etude de stabilité de l'édifice ». 01-mai-2014.

- [14] J. F. Lagneau, « Ancienne abbaye Saint Martin, réfectoire, Investigations visuelles », 3327, 2006.
- [15] L. Buffo-Lacarrière, A. Sellier, A. Turatsinze, and G. Escadeillas, « Finite element modelling of hardening concrete: application to the prediction of early age cracking for massive reinforced structures », *Mater. Struct.*, vol. 44, n° 10, p. 1821-1835, déc. 2011.
- [16] A. Hillerborg, M. Modéer, and P.-E. Petersson, « Analysis of crack formation and crack growth in concrete by means of fracture mechanics and finite elements », *Cem. Concr. Res.*, vol. 6, n° 6, p. 773-781, nov. 1976.
- [17] A. D. Jefferson and T. Bennett, « Micro-mechanical damage and rough crack closure in cementitious composite materials », *Int. J. Numer. Anal. Methods Geomech.*, vol. 31, n° 2, p. 133-146, 2007.
- [18] S. Kahraman, « Evaluation of simple methods for assessing the uniaxial compressive strength of rock », *Int. J. Rock Mech. Min. Sci.*, vol. 38, n° 7, p. 981-994, 2001.
- [19] Z. Moradian and M. Behnia, « Predicting the Uniaxial Compressive Strength and Static Young's Modulus of Intact Sedimentary Rocks Using the Ultrasonic Test », *Int. J. Geomech.*, vol. 9, n° 1, p. 14-19, 2009.
- [20] T. Parent, « Méthodologie de diagnostic de structures maçonnées anciennes », phd, Université de Toulouse, Université Toulouse III - Paul Sabatier, 2015.
- [21] Y.-M. Froidevaux, *Techniques de l'architecture ancienne: construction et restauration*. Editions Mardaga, 2001.

- [22] N. Domede, « méthode de requalification des ponts en maçonnerie », Thèse, Toulouse II, 2006.
- [23] J.-M. Laurent, *Construction et restauration des bâtiments en pierre*. Editions Vial, 2007.
- [24] NF EN 459, *Chaux de construction*, AFNOR. 2012.
- [25] NF EN 1015-11, *Méthodes d'essai des mortiers pour maçonnerie, partie 11, Détermination de la résistance en flexion et en compression du mortier durci*, AFNOR. 2000.
- [26] N. Domede, A. Sellier, and T. Stablon, « Structural analysis of a multi-span railway masonry bridge combining in situ observations, laboratory tests and damage modelling », *Eng. Struct.*, vol. 56, p. 837-849, nov. 2013.
- [27] T. Stablon, A. Sellier, N. Domede, B. Plu, and L. Dieleman, « Influence of building process on stiffness: numerical analysis of a masonry vault including mortar joint shrinkage and crack re-closure effect », p. 881-898, 2012.
- [28] NF EN 1052-1, *Méthodes d'essai de la maçonnerie*, AFNOR. 99.

**Figure 1.** Architecture of the monument : Outside view (a), inside view (b), longitudinal cross section view (c) transversal cross section view (d) [13], plan view (e) [14]

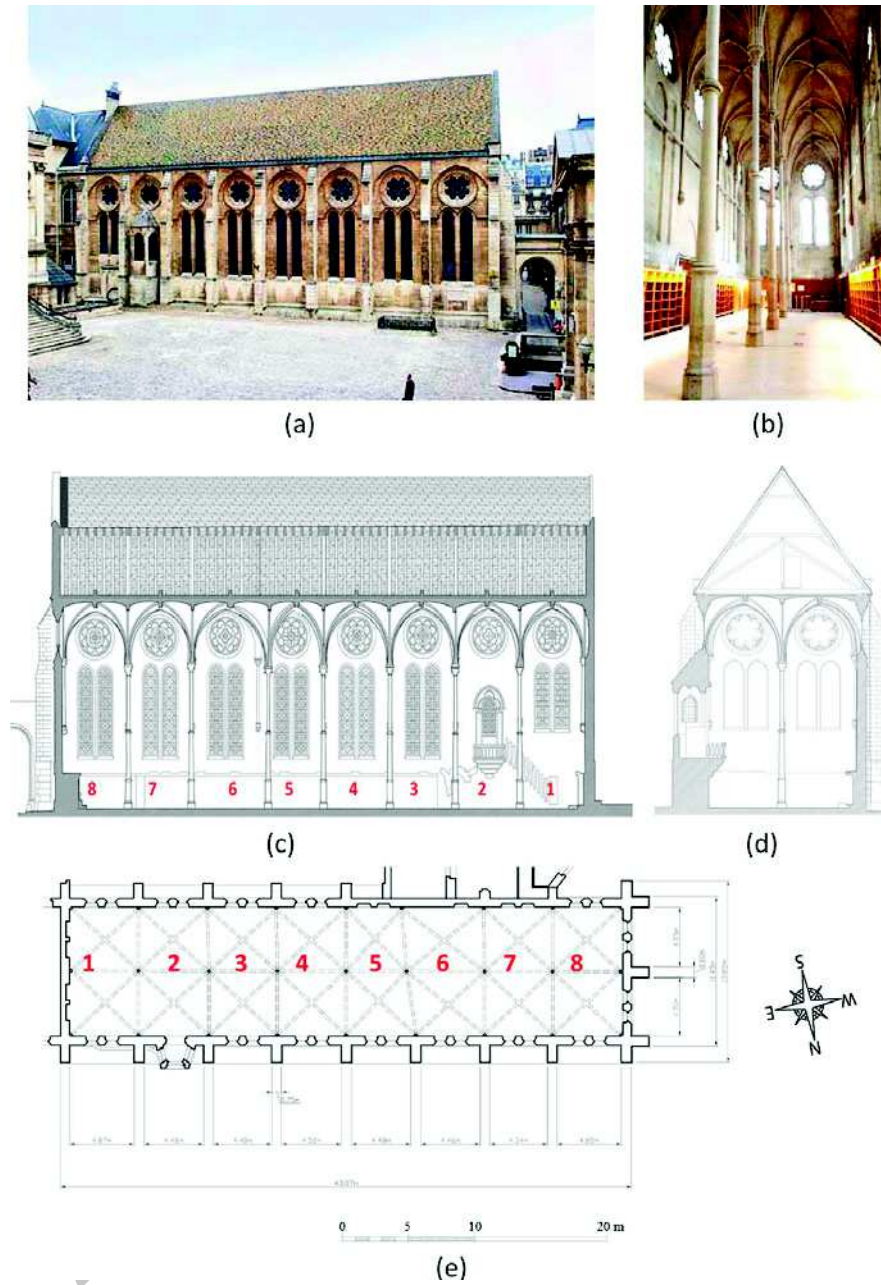
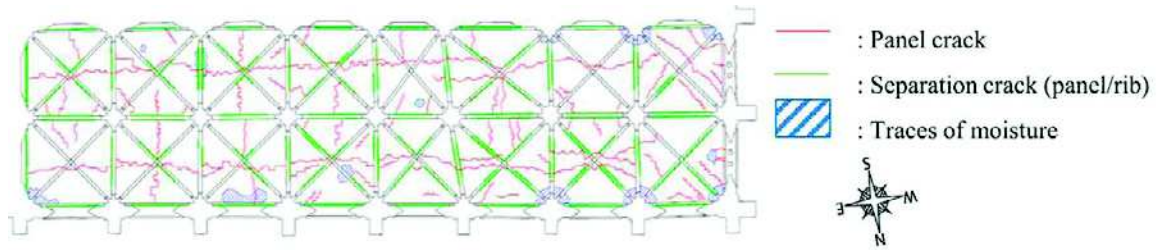


**Figure 2.** Crack pattern at the ribbed-vault intrados



Accepted Manuscript

**Figure 3.** Different masonries in place in the monument: (a) elevation wall, (b) ribbed-vault

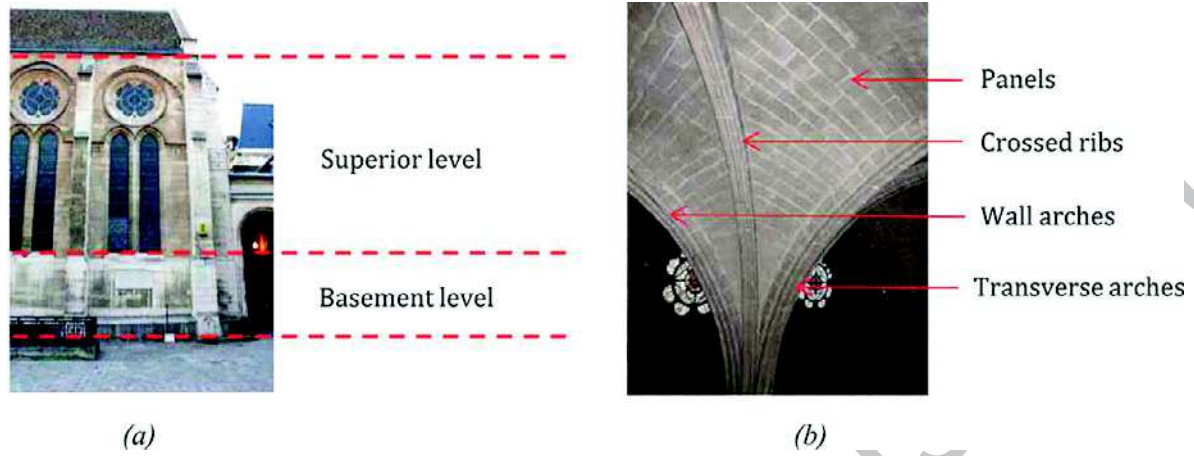
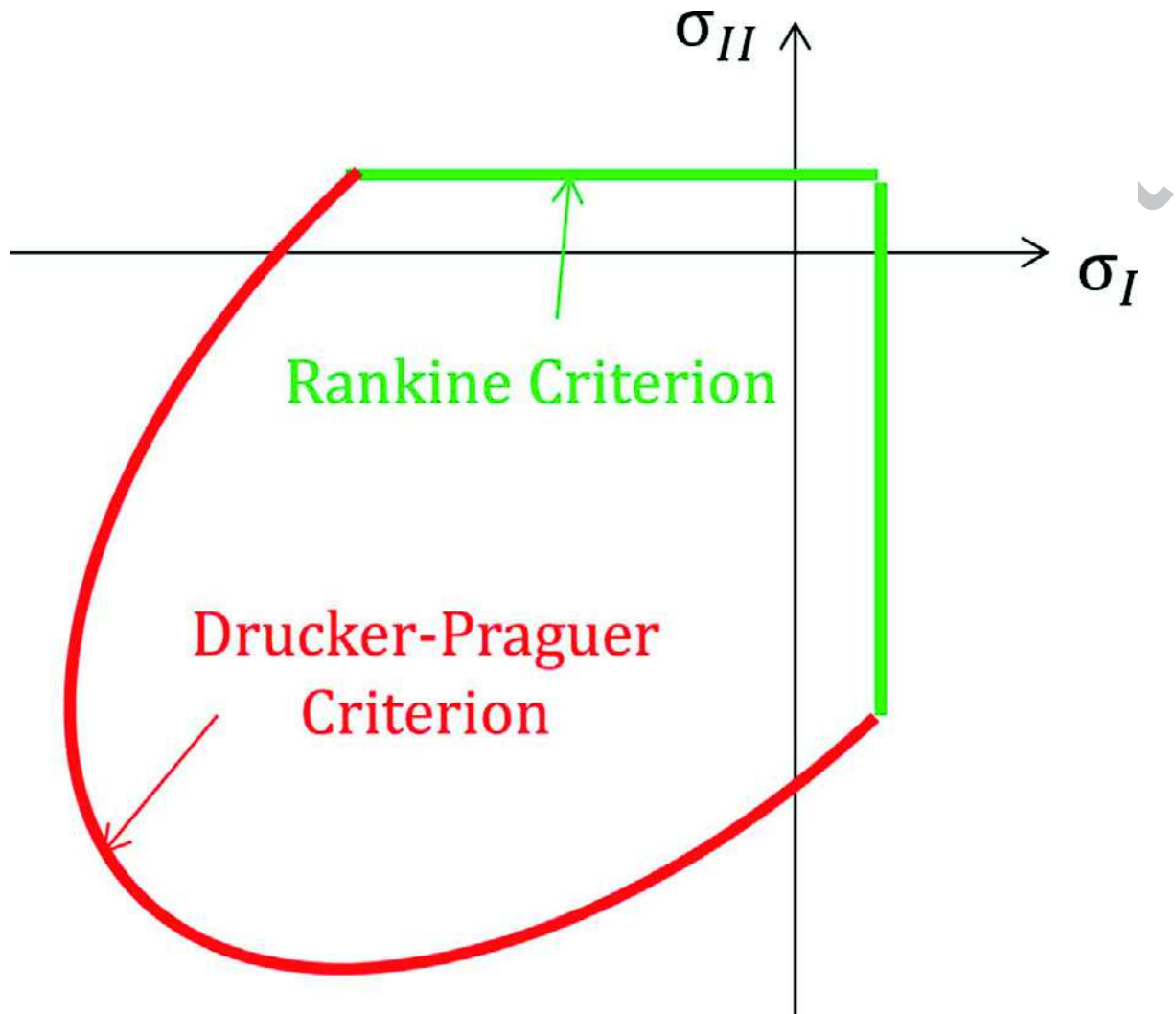
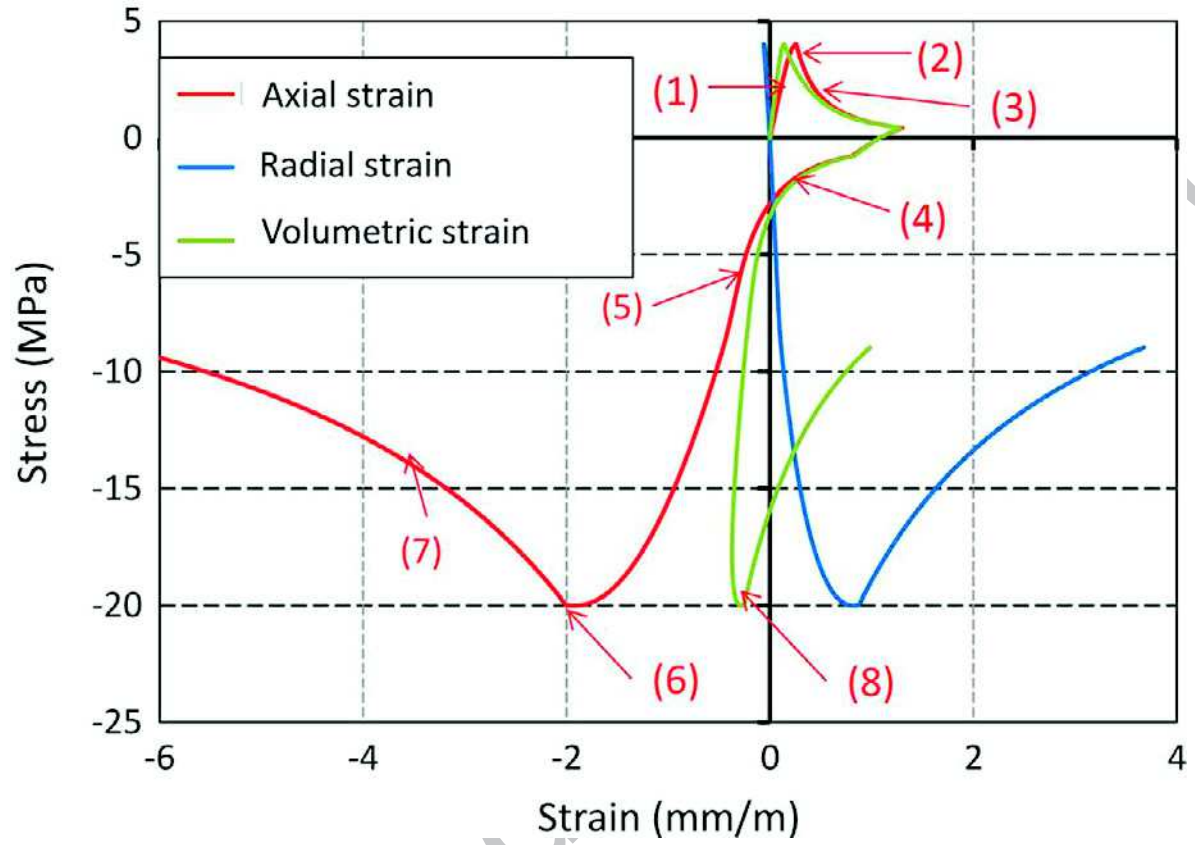


Figure 4. Plastic criteria in principal stresses base



ACCEPTED

Figure 5. Stress-strain law of the orthotropic damage model in tension and compression



**Figure 6.** Representative elementary volume (REV) of masonry according to European standards[28]

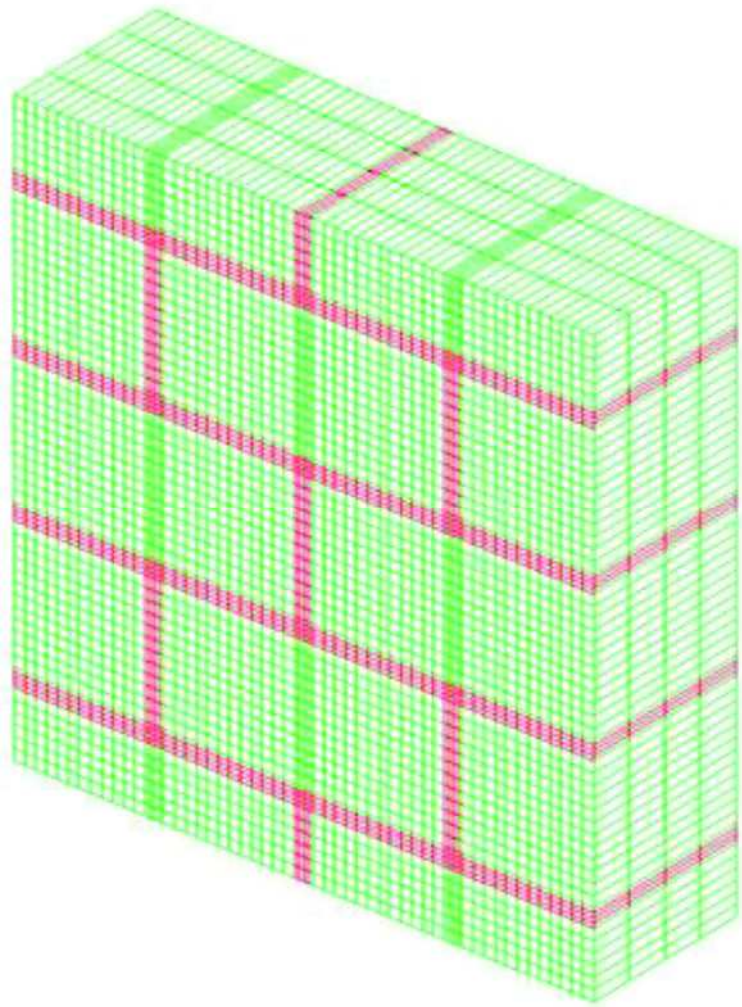
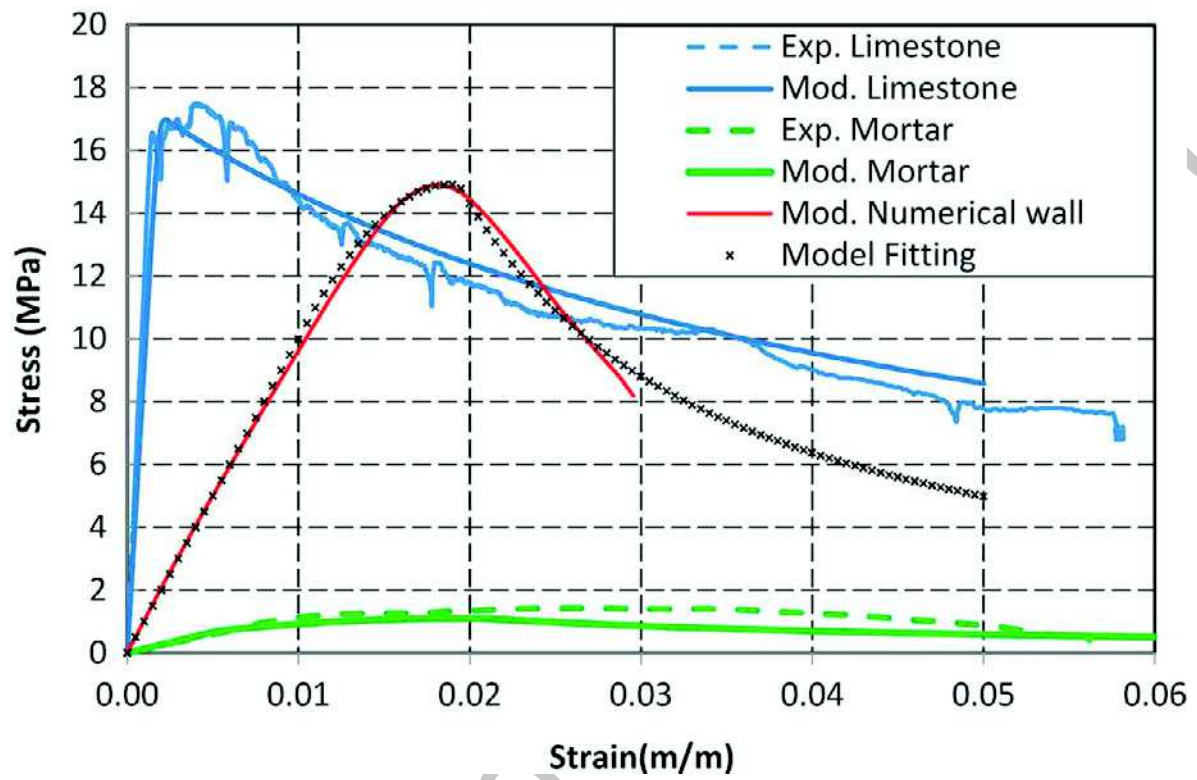
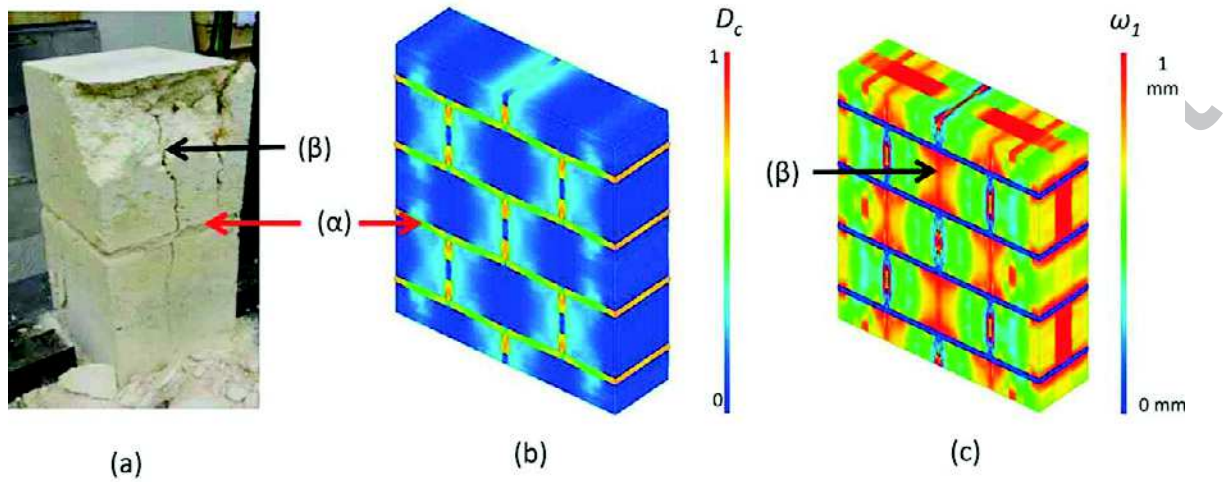


**Figure 7.** Experimental and numerical stress-strain relationship in compression for limestone, mortar and homogenized material



Accepted

**Figure 8.** Failure mechanism of masonry in compression (a) Composite sample of block-mortar-block after failure, (b) Compressive damage at the failure of the REV, (c) Crack opening at the failure of the REV

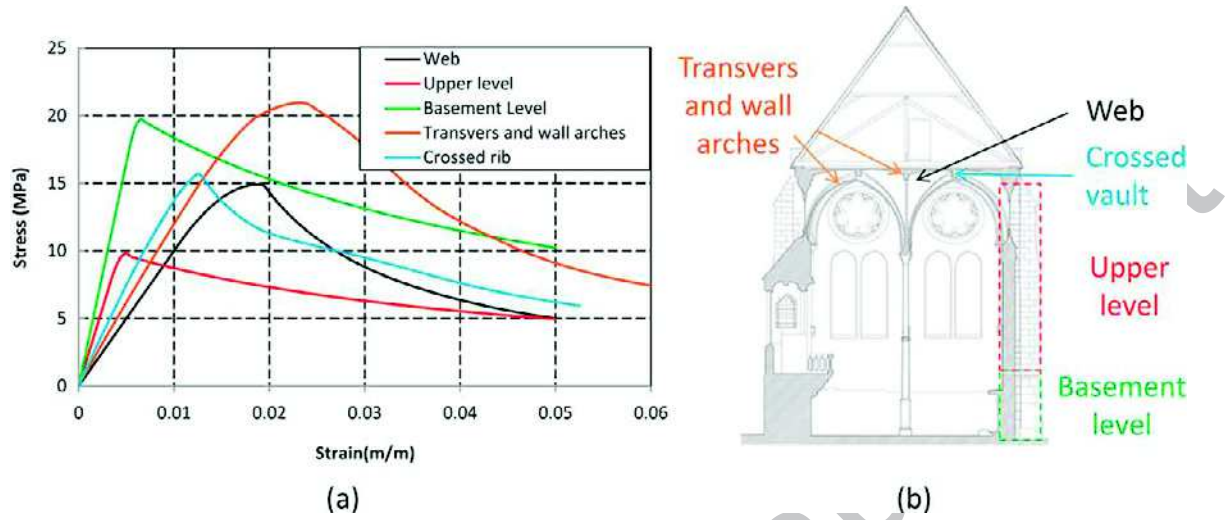


**Legend:**

- (α): Peripheral area of unconfined mortar
- (β): Vertical crack on limestone blocks

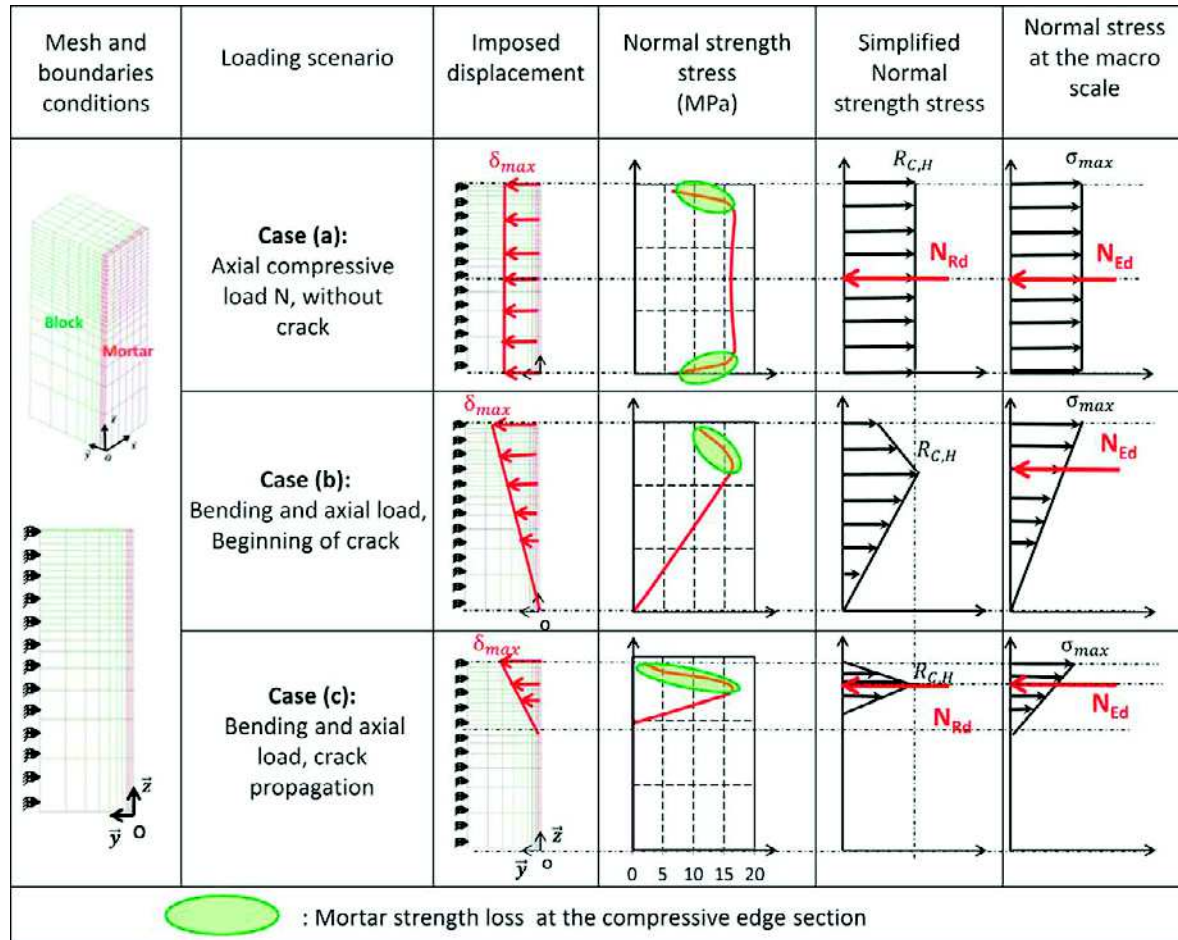
Accepted Manuscript

Figure 9. Stress-strain relationship in compression of homogenised masonries per zone



Accepted Manuscript

Figure 10. Analysis of a masonry section under different type of loading



**Figure 11.** Compressive damage in mortar at failure for the 3 cases of loading. Identification of the peripheral area of unconfined mortar

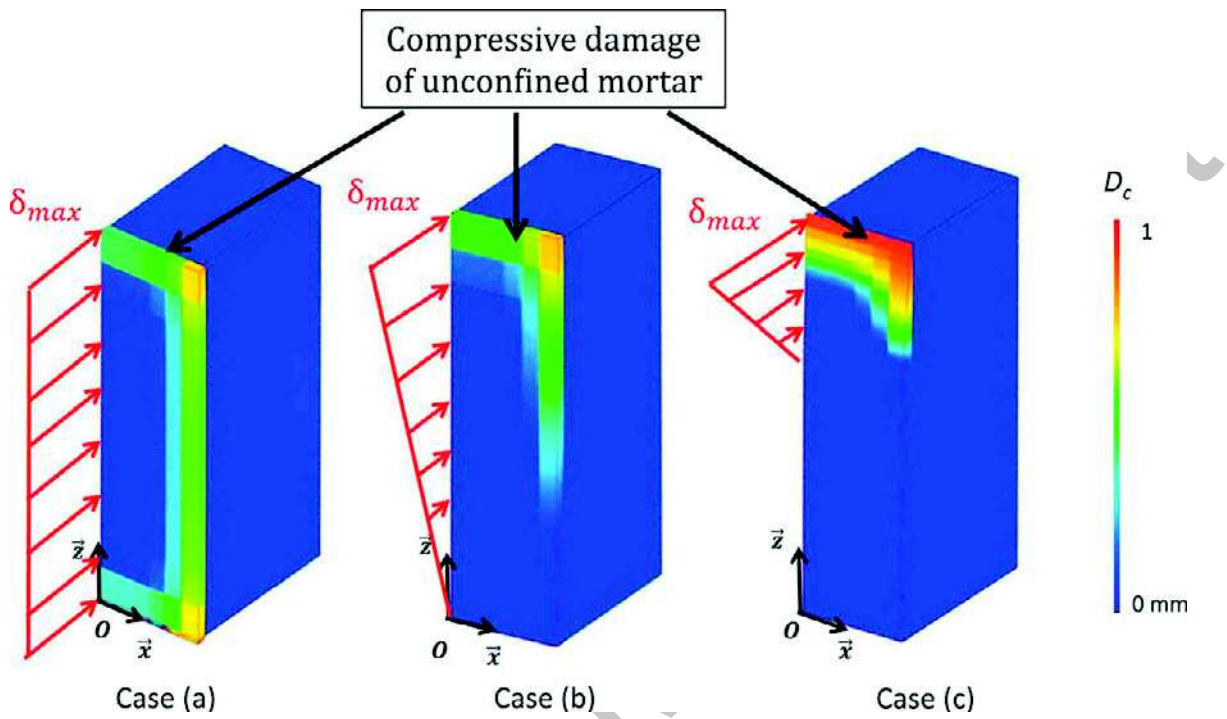


**Figure 12.** Simplified modelling of a bay of the refractory and mechanism connected with the removal centering formwork

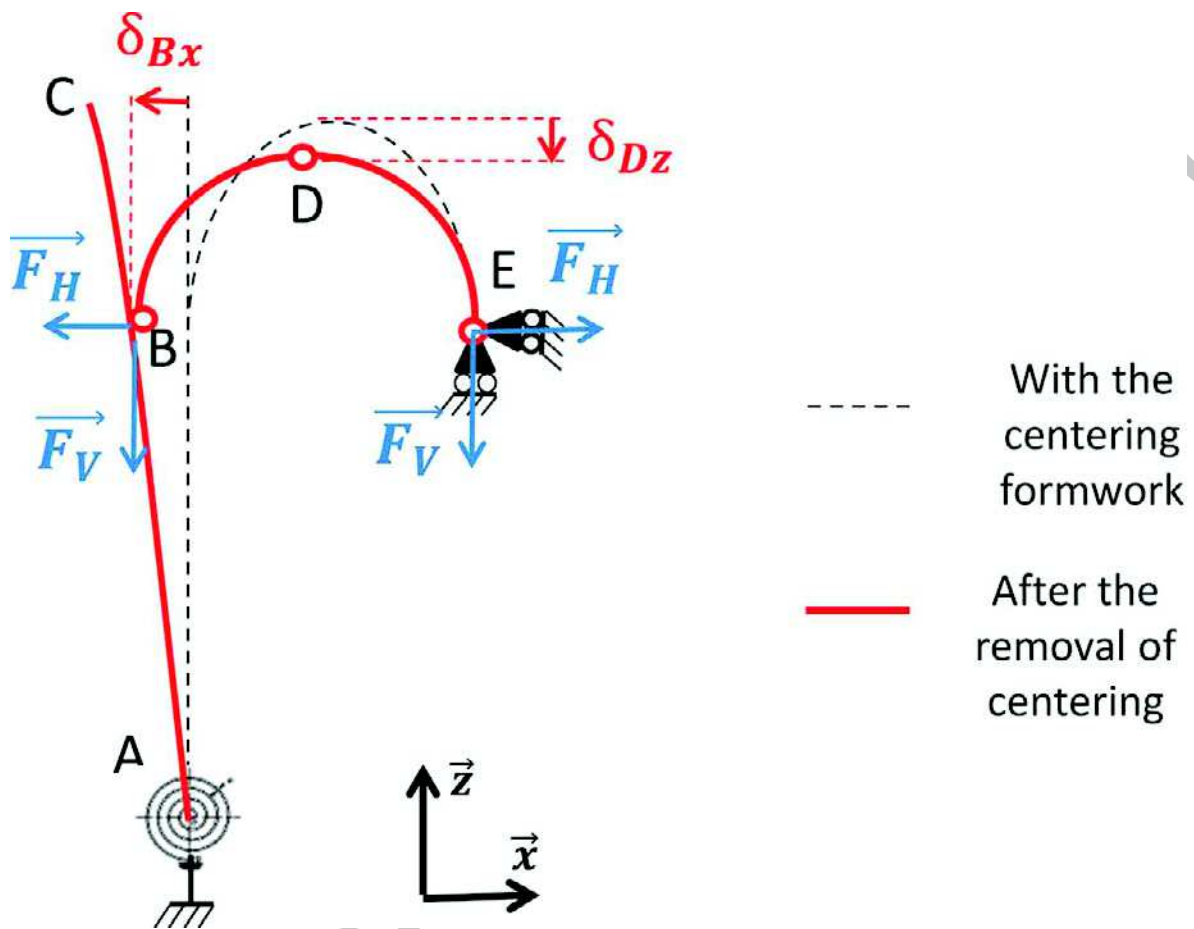
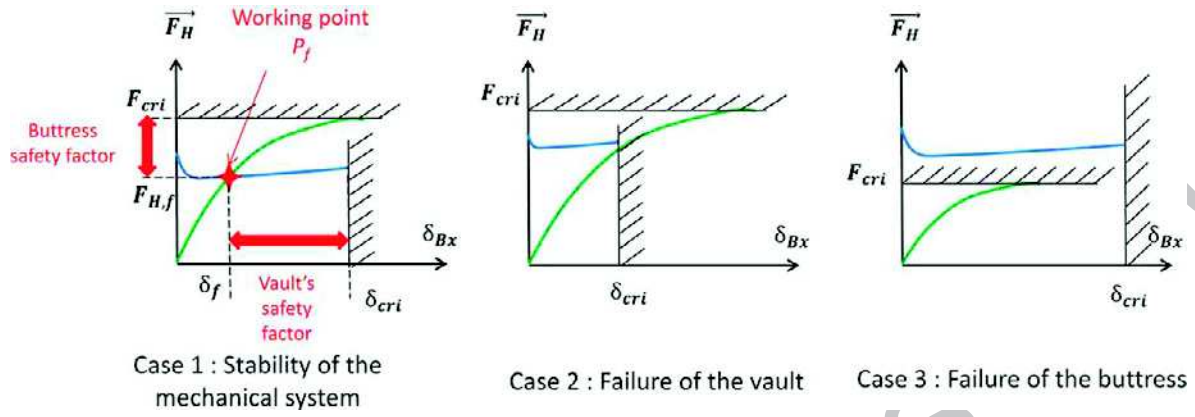
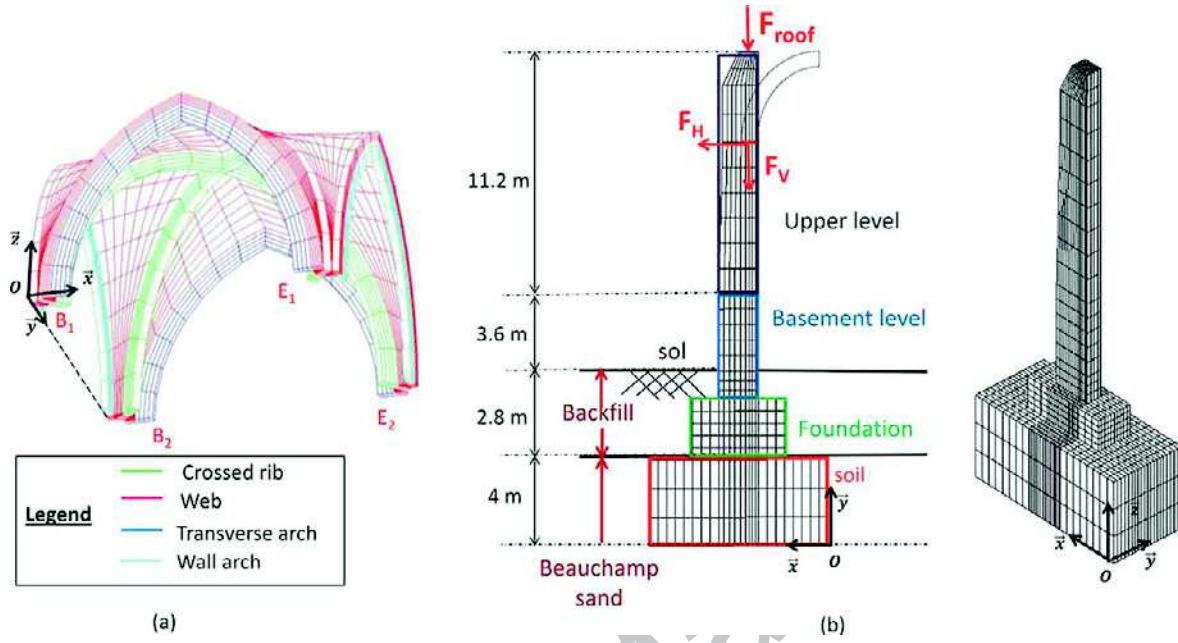


Figure 13. Different scenarios of stability of the mechanical system



Accepted Manuscript

Figure 14. FEM Mesh, (a) Ribbed vault, (b) Buttress



Accepted Manuscript

Figure 15. Behaviour law of the ribbed vault, Horizontal load vs Horizontal displacement

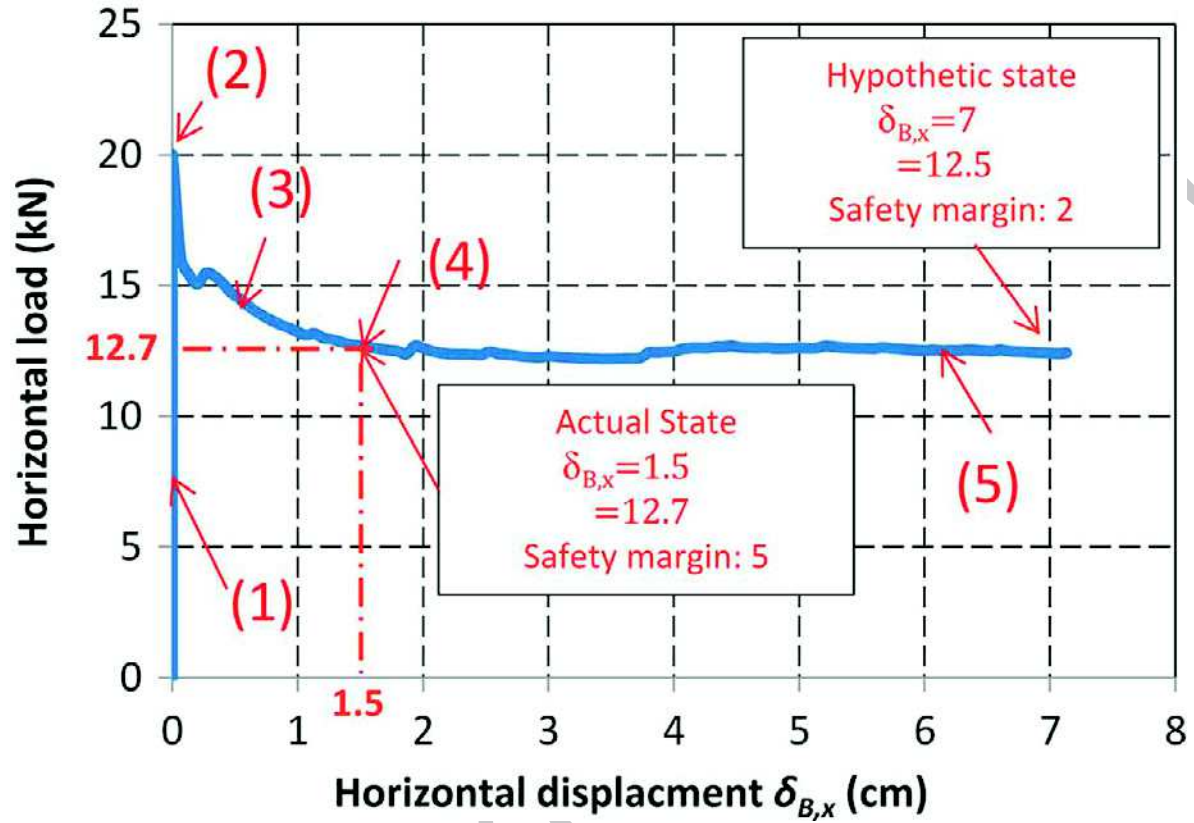


Figure 16. Crack opening for a displacement  $\delta Bx$  of about 1.5 cm

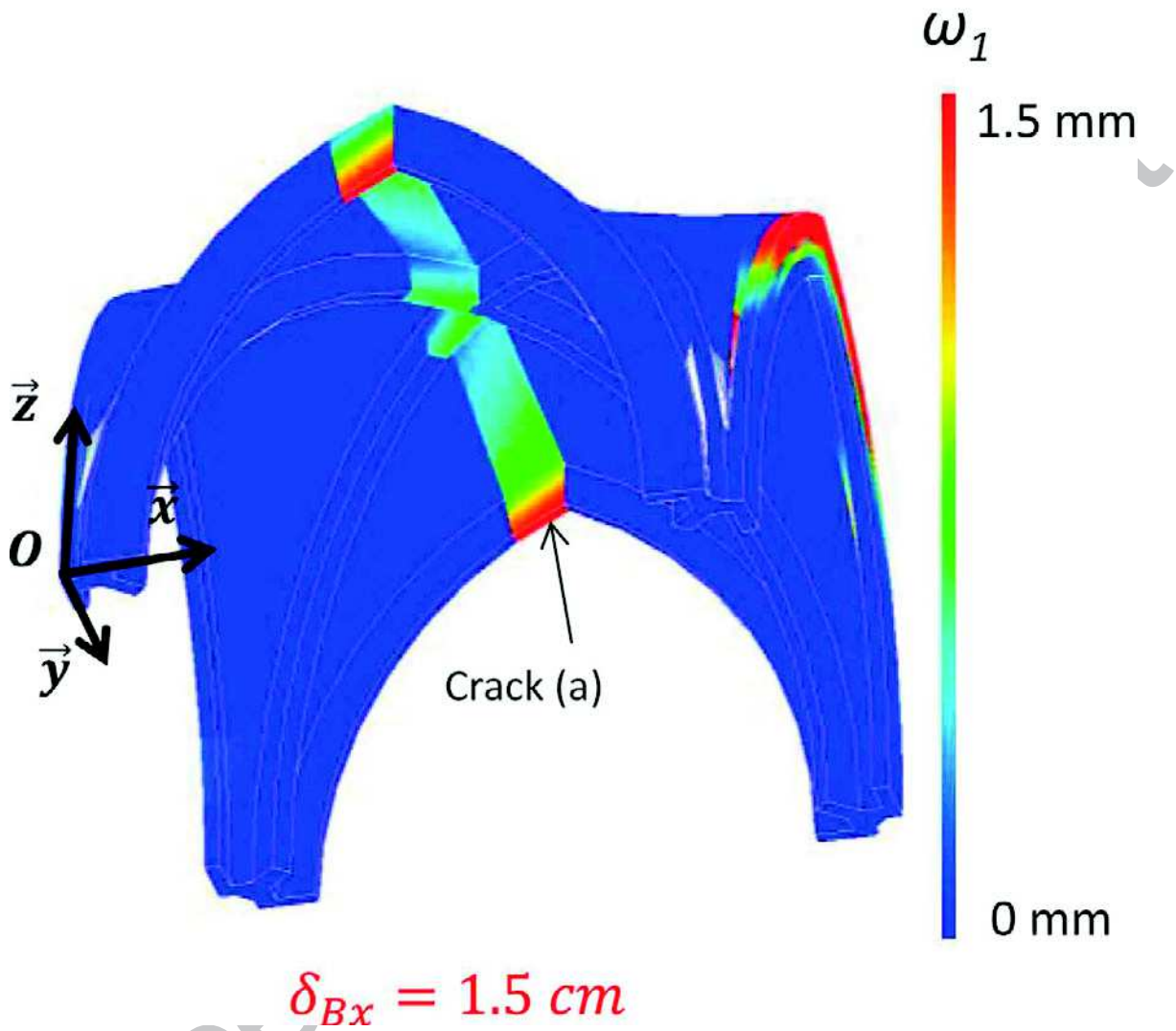
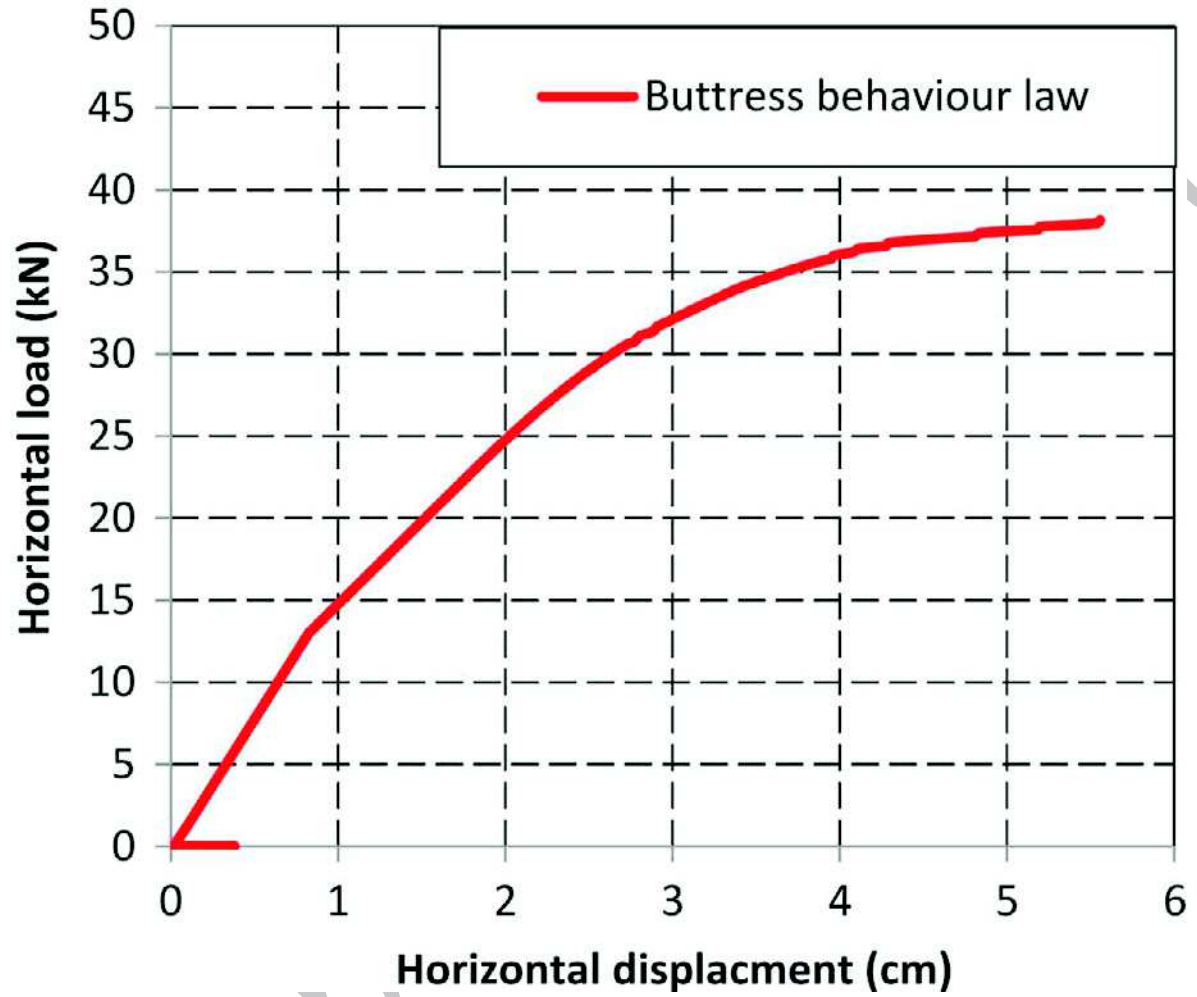


Figure 17. Behaviour law of the buttress, Horizontal load vs Horizontal displacement



Accepted

Figure 18. Crack opening at the real loading ( $F_H = 12.7 \text{ kN}$ )

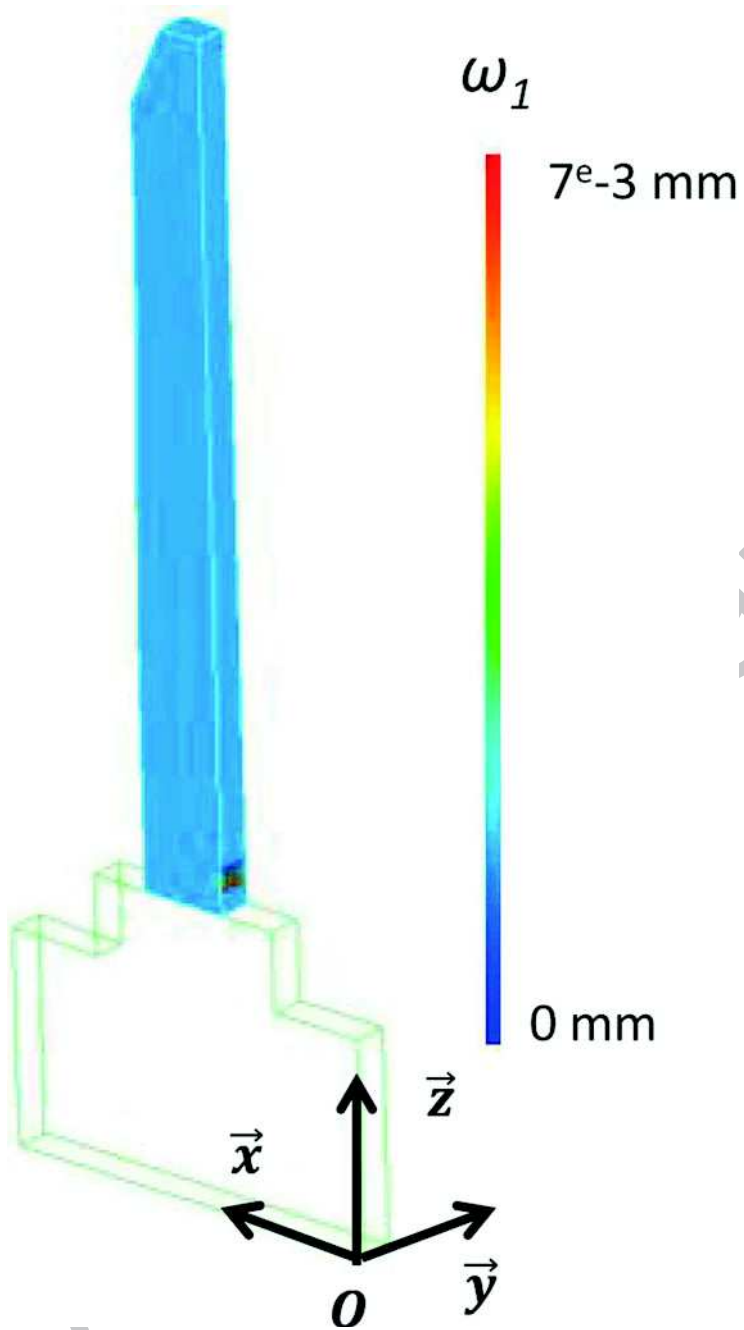


Figure 19. Stability assessment of the library bay

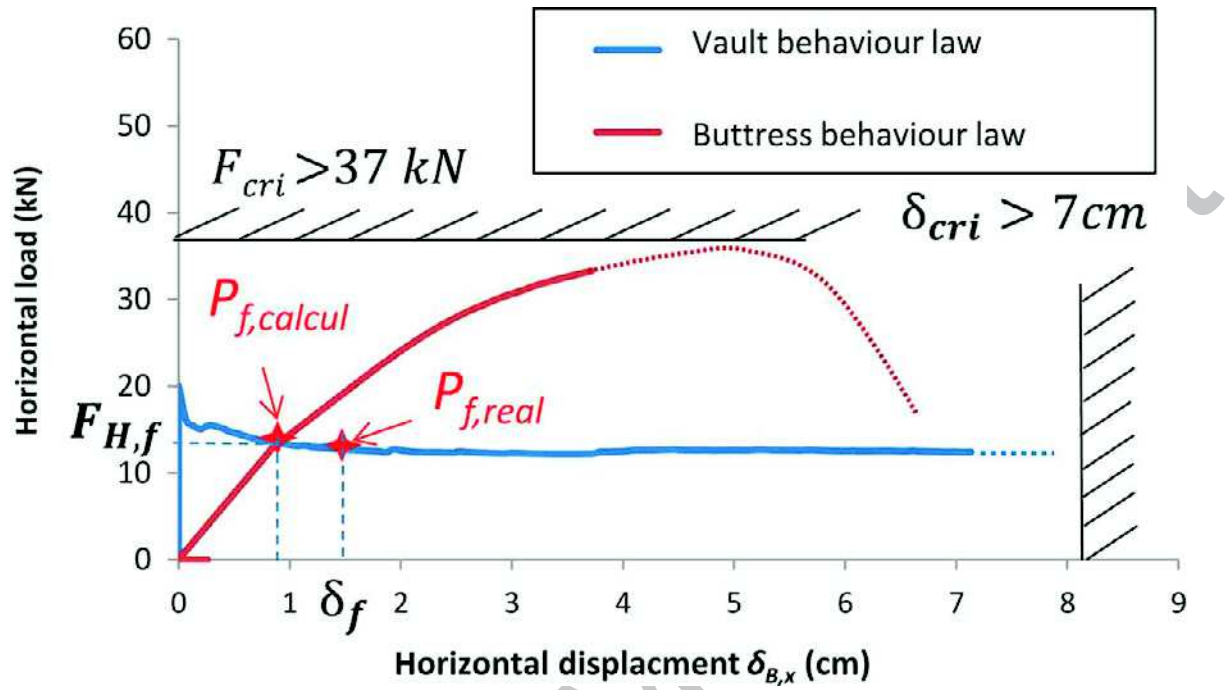
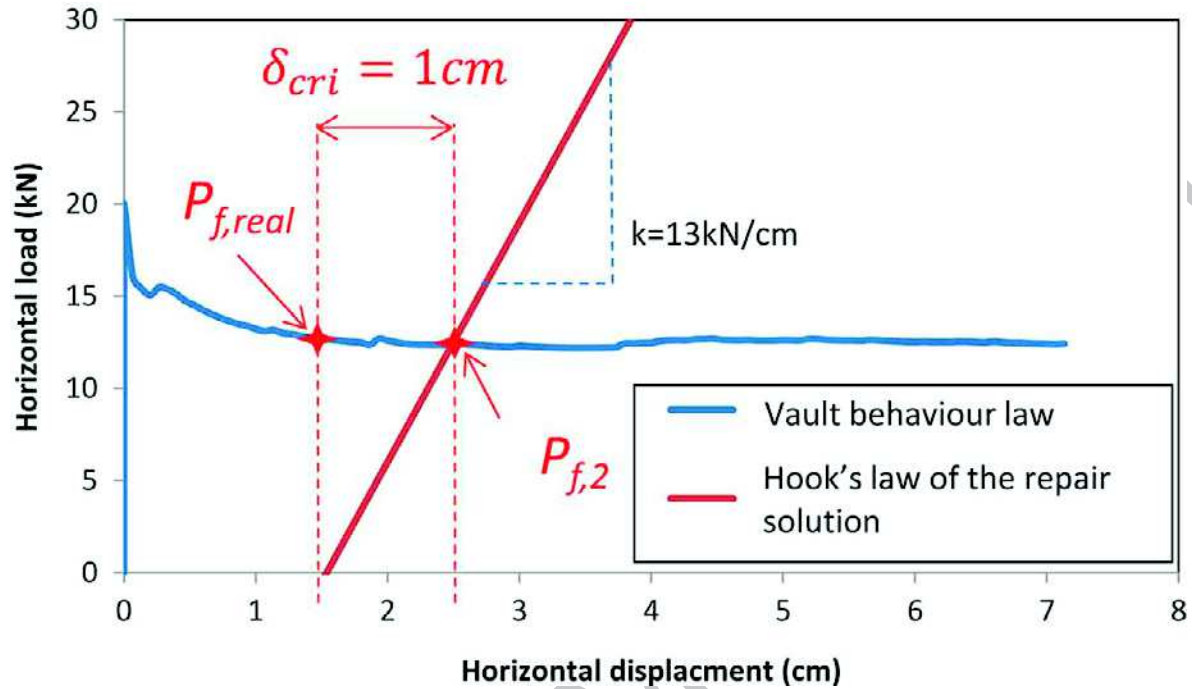


Figure 20. Design of the strengthening solution



Accepted Manuscript

Table 1. Velocity measurements of ultrasonic wave propagation in limestone, average and standard deviation

<b>Ultrasonic wave propagation (m/s)</b> $V_p$	<b>Basement level</b>	<b>Upper level</b>	<b>Panels</b>	<b>Crossed ribs</b>	<b>Transverse and wall arches</b>
<b>Number</b>	13	9	4	3	3
<b>Average(m/s)</b>	2966	2313	2774	2722	3076
<b>Standard deviation (%)</b>	25%	29%	9%	7%	8%

Table 2. Mechanical properties of limestones blocks

	<b>Basement level</b>	<b>Upper level</b>	<b>Webs</b>	<b>Crossed rib</b>	<b>Transverse and wall arches</b>
<b><math>\rho</math> (kg/m<sup>3</sup>)</b>	2002	1767	1939	1921	2037
<b><math>E</math> (GPa)</b>	10.9	6.2	9.3	9.0	11.8
<b><math>\nu</math></b>	0.22	0.20	0.22	0.21	0.22
<b><math>R_c</math> (MPa)</b>	20	10	17	16	22
<b><math>R_t</math> (MPa)</b>	5.0	2.4	4.3	4.1	5.4

Table 3. Mechanical properties of equivalent mortars

<b>Mechanical properties of equivalent mortars</b>	<b><math>\rho</math> (kg/m<sup>3</sup>)</b>	<b><math>E</math> (GPa)</b>	<b><math>\nu</math></b>	<b><math>R_c</math> (MPa)</b>	<b><math>R_t</math> (MPa)</b>
	1640	150	0.2	1.1	0.6

Accepted Manuscript